LETTERS
https://doi.org/10.1038/s41558-020-0753-9

nature climate change

Check for updates

Synchronized tropical Pacific and extratropical variability during the past three decades

Jun-Chao Yang[1,2], Xiaopei Lin[1,2]✉, Shang-Ping Xie[3], Yu Zhang[1,2,3], Yu Kosaka[4] and Ziguang Li[1,2]

Internally generated decadal variability influences global mean surface temperature (GMST), inducing acceleration and slowdown of the warming rate under anthropogenic radiative forcing[1–4]. While tropical eastern Pacific variability is important for annual-mean GMST[2,5–8], the cold ocean–warm land (COWL) pattern[9,10] also contributes to continental temperature variability[11–13] in the boreal cold season. Although the two contributors are physically independent[10,12], here we show that, after the mid-1980s, their decadal components vary in phase by chance to strengthen internal GMST trends, contributing to the early 2000s slowdown and early 2010s acceleration. The synchronized tropical Pacific and COWL variability explains the striking seasonality of the recent slowdown and acceleration during which the GMST trend in the boreal cold season is markedly negative and positive, respectively. Climate models cannot simulate the exact timing of the tropical Pacific and COWL correlations because they are physically independent, random-phased modes of internal variability.

The rate of global warming exhibits decadal slowdown and acceleration. Although defined on annual-mean global mean surface temperature (GMST) trends, the slowdown and acceleration events display distinctive seasonal and regional characteristics. They are associated with, for example, regional temperature anomalies[14], drought[5] and extremes[15]. While problems in estimating GMST[16] and radiative forcing[17] complicate the attribution of slowdown and acceleration events, internal variability of the climate system is important, with distinctive seasonal and regional features. Here, we remove the model-estimated radiative GMST (Supplementary Fig. 1) from raw observed data[7] and treat the residual as the internal component (Methods).

During four recent decades, three acceleration and slowdown events have occurred: the 1975–1998 acceleration, the 2002–2013 slowdown and the 2008–2017 acceleration (Methods). In the boreal cold season (November to the following March) of the recent slowdown, the internally driven surface temperature trend pattern (Fig. 1b) features cooling over the tropical eastern Pacific (TEP) and Northern Hemispheric continents. The cooling in the TEP is associated with global-scale atmospheric teleconnection and regional ocean circulation changes[5–8], while Northern Hemispheric continents are forced by mid-latitude atmospheric circulation patterns[12,13]. Model simulations show that the North American cooling is induced in part by the tropical Pacific cooling[5,12,14]. Here we show that similar temperature anomalies (with reversed sign) appeared over the TEP and Northern Hemispheric continents during the other two acceleration events (Fig. 1a,c). For annual-mean GMST variability, the TEP is a major pacemaker[2]. In the boreal cold season, however, the continental signals are also important for GMST variability. We show that the synchronization between the TEP and continental variability strongly enhances internal GMST trends.

We use a cold ocean–warm land (COWL) index to track Northern Hemispheric continental temperature variations[9,18]. The original definition of the index is based on raw data and includes both internally generated variability and anthropogenic fingerprints[19]. Here we define the COWL index based on the internal variability (Methods). The COWL pattern features cold Eurasia and western North America, and warm northeastern North America and Greenland in its negative phase. The COWL contribution matches the continental temperature trends in the recent slowdown and acceleration events well (Fig. 1b,c), while the match is not as good for the 1975–1998 acceleration (Fig. 1a). These COWL-like temperature trend patterns extend their general structure into the lower troposphere north of 30°N (contours in Supplementary Fig. 2). We also use the tropical Pacific index[20] (TPI) to track TEP internal sea surface temperature variability (Methods). The COWL index is independent of the TPI with a negligible correlation coefficient of −0.04 over 1921–2018. This permits us to use a two-variant linear regression method to estimate the contributions of the COWL and TPI for internal GMST variability (Methods).

Using the time span of each acceleration/slowdown event as the running window, we calculate the TPI- and COWL-related GMST trends in the boreal cold season (Fig. 1d and Supplementary Figs. 3a,c). While the two vary independently for most of the twentieth century, a striking synchronization emerges after the mid-1980s, with both featuring large excursions at the timing of the three acceleration/slowdown events. Hereinafter, we call each running trend a segment. The 30-segment running correlation between the TPI- and COWL-related GMST trends is weak in much of the record but reaches high positive values in recent decades (Fig. 1e and Supplementary Figs. 3b,d). The correlation values of the recent 30-segment period exceed the 95th percentile in climate model ensembles (Methods), with some variabilities among different ensembles (Supplementary Table 1). For all the model samples, the observed correlations generally exceed the 95th percentile after the mid-1980s and exceed the 99th percentile more recently (Fig. 1e and Supplementary Figs. 3b,d).

The synchronization between the TEP and COWL variability in the past three decades is mainly a coincidence. Although some studies suggested potential physical linkages between the Pacific and tropospheric temperature in the Northern Hemisphere[21], they are mostly independent at the surface over large areas of Eurasia[2,9–12]

[1]Frontiers Science Center for Deep Ocean Multispheres and Earth System and Physical Oceanography Laboratory, Ocean University of China, Qingdao, China. [2]Qingdao National Laboratory for Marine Science and Technology, Qingdao, China. [3]Scripps Institution of Oceanography, University of California San Diego, La Jolla, CA, USA. [4]Research Center for Advanced Science and Technology, University of Tokyo, Tokyo, Japan. ✉e-mail: linxiaop@ouc.edu.cn

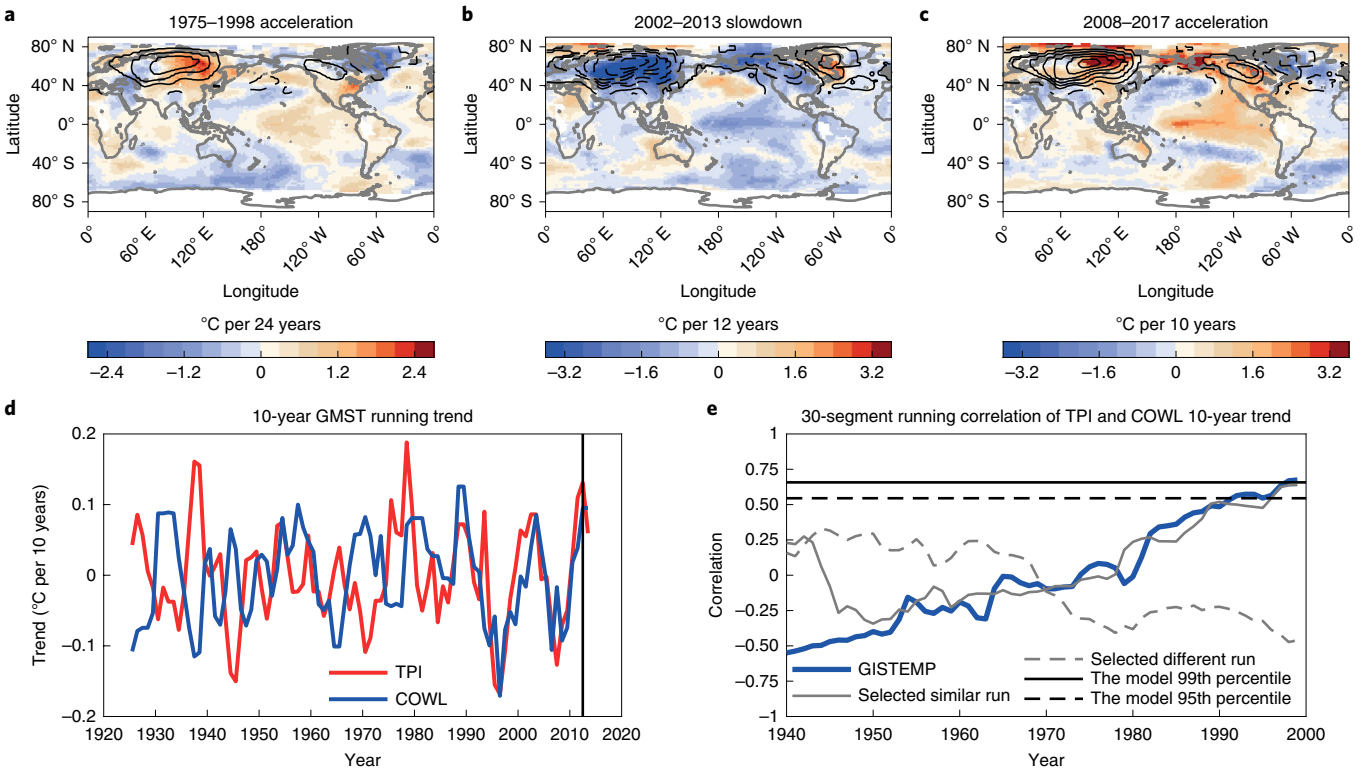

Fig. 1 | TEP–COWL synchronization. a–c, Internal surface temperature trend patterns (colour-shaded) during the 1975–1998 acceleration, 2002–2013 slowdown and 2008–2017 acceleration events, respectively. COWL contribution is denoted by black contours with an interval of 0.25 °C per 24 years (**a**), 0.5 °C per 12 years (**b**) and 0.5 °C per ten years (**c**). Positive and negative contributions are shown by solid and dashed lines, respectively, and the zero line is omitted. **d**, Ten-year running trends of TPI-related (red) and COWL-related (blue) GMST. The TPI-related trend is divided by two for display purposes. Years denote the centre time of a trend segment. The vertical line denotes the timing of the 2008–2017 acceleration. **e**, The 30-segment running correlation (blue line) of ten-year running trends of TPI and COWL indices. Years denote the centre time of the 30-segment window. Selected model runs in CESM1 large ensemble similar to and different from observations are shown by grey solid and dashed lines, respectively. Horizontal solid and dashed lines denote the model-estimated 99th and 95th percentiles, respectively.

(Fig. 2a–d). In a TEP-pacemaker ensemble simulation, a member run captures Eurasian cooling during 2002–2013 winters much as in observations, but this feature is independent of the TEP force and indeed absent in the ensemble mean[12]. Specifically, an atmospheric model forced by historical ocean boundary conditions (including sea surface temperature and sea-ice) fails to track continental temperature trends (Fig. 2e,f), suggesting that the COWL variability mainly arises from atmospheric internal dynamics[11,12]. A caveat is that such experiments generally underestimate sea-ice forcing[22]. In models, the TEP plays a minor role in driving COWL decadal variability. Community Earth System Model 1 (CESM1) runs with only minor differences in initial conditions exhibit very different histories of the correlation between the TPI and COWL indices, confirming the random nature of their correlation (Supplementary Fig. 4; CM2.1 confirms the results but is not shown). In a CESM1 historical experiment[23], as an example, some members show correlation time series very similar to the observed one, but some show totally different histories (Fig. 1e and Supplementary Figs. 3b,d).

The shift in TPI–COWL correlation is accompanied by distinctive spatial characteristics. Before the shift, the correlations between the TPI and internal surface temperature decadal trends are strongly positive only in North America (Supplementary Fig. 5a), in accordance with the conventional TEP-forced pattern[14]. At the same time, the decadal trends of the COWL index show minor correlations with temperature trends in the TEP (Supplementary Fig. 5c). By contrast, the correlation pattern with the TPI in recent decades projects well onto the COWL pattern (Supplementary Fig. 5b). Quantitative assessments on temperature advections (Supplementary Fig. 6) suggest that the positive correlations in Eurasia are dynamically forced by a low-pressure centre to the north (30°E–180°, north of 60°N, Supplementary Fig. 5b): anomalous northwesterly winds on the southwestern rim of the low-pressure centre warm the land over Siberia by advecting climatologically warmer oceanic air. The COWL correlation pattern in the TEP region projects well onto the tropical signal of the Interdecadal Pacific Oscillation[24] (Supplementary Fig. 5d). The TPI–COWL correlation shift is more obvious when using ten-year low-pass filtered time series (Methods) instead of running trends (Supplementary Fig. 7).

Although a wintertime phenomenon, the TEP–COWL synchronization results in strong modulations of annual-mean internal GMST trends. To assess GMST contribution of the TEP–COWL synchronization, the cold season TPI- and COWL-related GMST trends (Fig. 1d and Supplementary Figs. 3a,c) are summed (denoted as TPI + COWL) and then regressed onto the annual-mean GMST trends. In observations, the TPI + COWL contributes to more than 40% standard deviation (s.d.) of annual-mean internal GMST trends over 24 years (Supplementary Fig. 8a). The TPI + COWL contribution increases to 60% for ten-year trends (Supplementary Fig. 8b).

Using CESM1 and Coupled Model Intercomparison Project 5 (CMIP5)[25] ensembles forced by historical radiative forcing, we further test the hypothesis that synchronized TPI–COWL variability, as measured by their contributions, intensifies annual-mean internal GMST trends during the recent 30-segment period. In both the model ensembles, the TPI–COWL correlations significantly

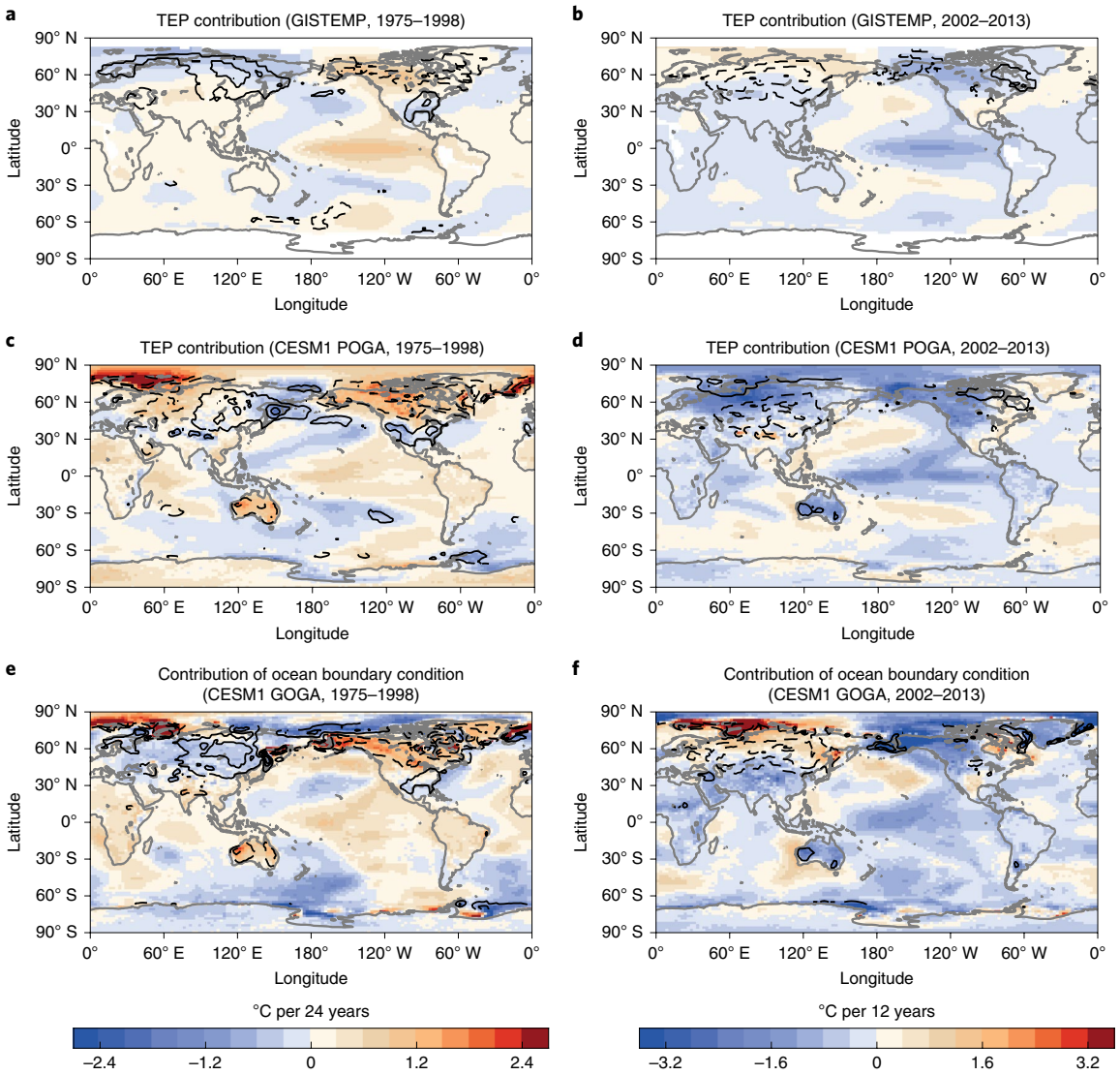

Fig. 2 | Observed Eurasian temperature trends independent of the TEP force. a,**c**,**e**, Internal surface temperature trends in the boreal cold season during 1975–1998 estimated by TPI-regressed contribution in the GISS Surface Temperature Analysis (GISTEMP) (**a**), the difference of CESM1 Pacific Ocean–Global Atmosphere (POGA) ensemble mean and historical ensemble mean (**c**) and the difference of CESM1 Global Ocean–Global Atmosphere (GOCA) ensemble mean and historical ensemble mean (**e**) (see Methods). **b**,**d**,**f**, As per **a**,**c**,**e**, but for 2002–2013. Patterns in **c**,**d** represent the contributions of the internal TEP-forced component, and patterns in **e**,**f** represent the internal contributions of sea surface temperature and sea-ice. The time of POGA and GOGA ensembles do not totally cover the recent acceleration, so this event is not analysed. The difference of observed internal surface temperature trend (Fig. 1a,b) and the estimated contribution of the TEP/ocean boundary condition (interpolated to observed grid points) is shown by contours in each panel. Positive and negative differences are shown by solid and dashed lines, respectively, with an interval of 1 °C per 24 years during 1975–1998 and 2 °C per 12 years during 2002–2013; the zero line is omitted. All panels exhibit strong differences, especially over Eurasia. The CM2.1 POGA run also fails to simulate observed Eurasian surface temperature trends (not shown).

correlate with the s.d. of annual-mean internal GMST ten-year trends (Fig. 3a), albeit with some ensemble spreads (Supplementary Fig. 8). The linear regression lines show that the trend s.d. more than doubles between the strongest positive (+1) and negative (−1) TPI–COWL correlations. For the extreme positive (Fig. 3b) and negative (Fig. 3c) internal GMST trends that are important for generating acceleration/slowdown events, the TPI–COWL correlation is still an important factor, but the relationship is weaker. The reason is that compared with s.d., the extreme trends feature much randomness, weakening the linear relationship. Observed values roughly ride on the model regression lines, implying that the observed TEP–COWL synchronization contributes importantly to extreme annual-mean internal GMST trends, hence the extreme acceleration and slowdown events. This relationship is similar for 12-year trends (not shown) but much weaker for 24-year trends (Supplementary Fig. 9). The Atlantic multidecadal variability dominates GMST variations on multidecadal timescales[4,26].

We further test how the boreal winter phenomenon (the TEP–COWL synchronization) can substantially modulate the annual-mean internal GMST decadal trends. In observations, the TPI + COWL contribution predominates internal GMST trends in the boreal cold season during three recent decades (Fig. 3d). The annual-mean internal GMST trend covaries with the wintertime one but is of weaker amplitudes because (1) the TEP effect on internal GMST variations is strong all year round but weakens in the warm season[2] and (2) the COWL effect only exists in the

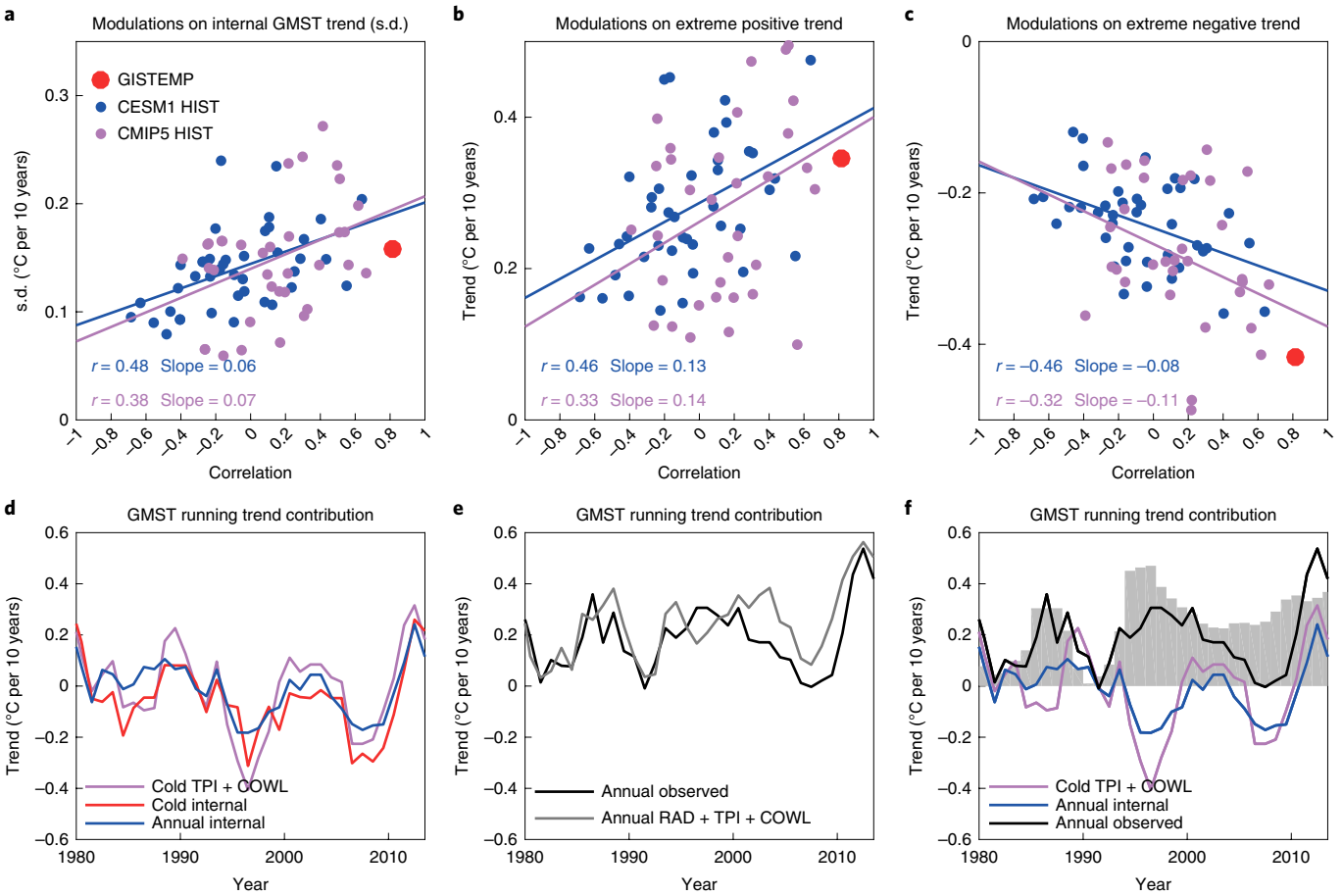

Fig. 3 | Modulations of TEP–COWL synchronization on internal GMST trends. a, The *x* axis denotes the recent 30-segment correlation of ten-year running trends of the TPI and COWL index, and the *y* axis denotes the s.d. of the recent 30-segment internal GMST trend. Observations (red dots), CESM1 historical (blue) and CMIP5 historical (purple) ensembles are shown. The regression line of each ensemble is also shown. Correlation (*r*) and regression (slope) coefficients are shown in bold type if exceeding the 95% significance test. HIST, historical. **b**,**c**, As per **a**, but the *y* axes denote extreme positive (**b**) and negative (**c**) trends of the recent 30-segment. **d**, Observed TPI + COWL GMST decadal trend in cold season (purple), internal GMST decadal trends in cold season (red) and for annual-mean (blue). **e**, Annual-mean GMST decadal trends (black), and the sum of radiative (RAD) and TPI + COWL contributions (grey). **f**, Some lines in **d**,**e** are repeated for comparison. The grey bar denotes the radiatively forced contribution.

cold season. Annual-mean GMST decadal trends are well tracked by the sum of the radiatively forced component and TPI + COWL contribution (Fig. 3e). Hence, the sign of the departure of GMST from radiative forcing is well tracked by the phase of the TPI + COWL contribution (Fig. 3f). As the TEP–COWL synchronization increases the possibility of extreme internal GMST trends (Fig. 3b,c), with a nearly constant rate of increase in the radiative forcing, this facilitates extreme slowdown and acceleration events.

The TEP–COWL synchronization does not guarantee the occurrence of an acceleration or slowdown event, even at the peak of the TPI + COWL contribution. As an example, in the mid-1990s, the TPI + COWL cooling effect is even stronger than that during the recent slowdown (Fig. 3f). However, a stronger warming effect from other internal variability and the strongest radiative warming during the recent decades prevent a slowdown event from occurring. Specifically, the strong radiative contribution results from the temperature recovery after the 1991 Mount Pinatubo eruption.

The TEP–COWL synchronization modulates the seasonality of acceleration/slowdown events[2,5,27–29]. The seasonality is dominated by internal variations as radiatively forced variability does not show large seasonal preference (Supplementary Fig. 1). In observations, the 1975–1998 acceleration shows no seasonality (Fig. 4a) while the recent decade-long events exhibit stronger trends in the boreal cold season (Fig. 4b,c). We turn to the 40-member CESM1 historical ensemble to examine whether TEP–COWL synchronization influences the seasonality. We calculate the annual-mean GMST trends during the same period of each observed acceleration/slowdown event in each ensemble member. Then, for each event, we sort the 40 members according to their annual-mean GMST trends: the top 50% members are sorted as acceleration events and the bottom 50% members as slowdown events. The correlation coefficients of the TPI and COWL trends are then calculated over the recent 30 segments. Based on the correlation, the top 50% acceleration/slowdown members are sorted into the high-synchronization group and the bottom 50% into the low-synchronization group.

For the 24-year acceleration of 1975–1998, high- and low-synchronization composites show no obvious difference (Fig. 4a). By contrast, composites for the decadal slowdown of 2002–2013 (Fig. 4b) and acceleration of 2008–2017 (Fig. 4c) exhibit large differences associated with the TEP–COWL synchronization. The dependency on trend duration arises in part from the Atlantic effect that increases with the trend period as mentioned before, and results in part from the fact that longer trends are dominated by external influence with weak seasonality (Supplementary Fig. 1). For decade-long events (Fig. 4b,c), observed events show even stronger seasonality than model composites. In January–March, the slowdown of 2002–2013

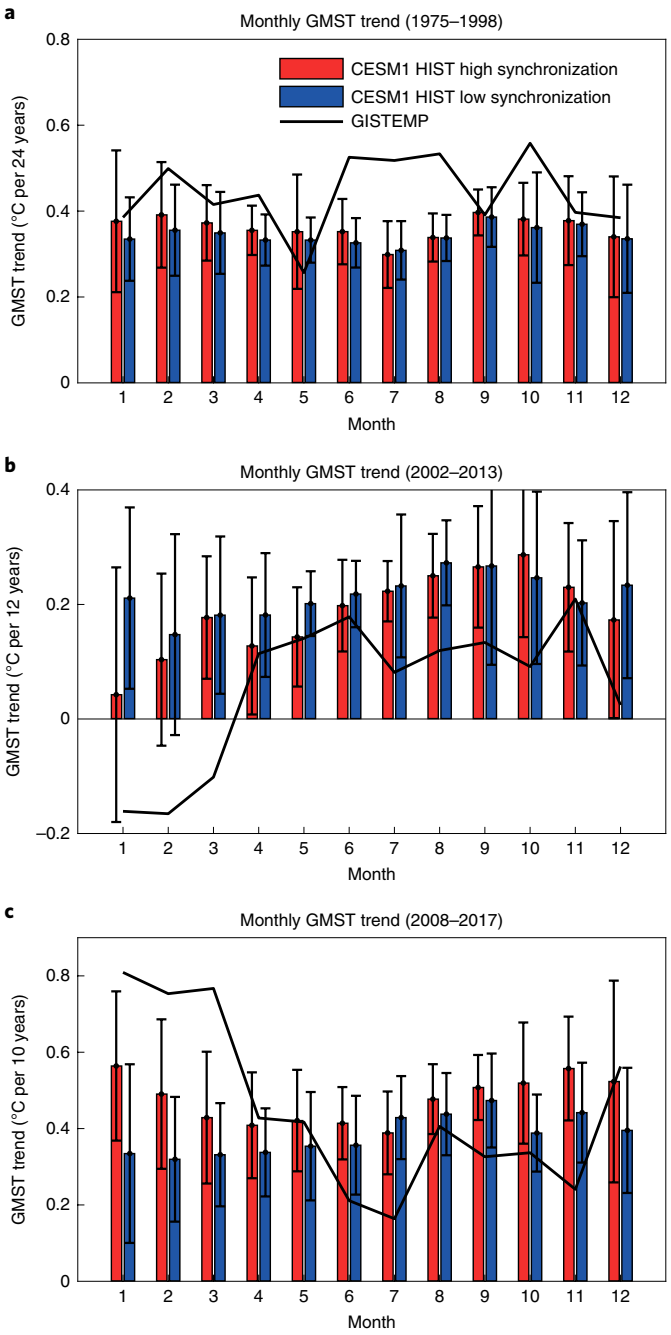

Fig. 4 | Seasonal modulations of TEP–COWL synchronization on acceleration/slowdown events. a, Observed GMST trends in each calendar month during the 1975–1998 acceleration (black line), and model composite for member runs of high (red) and low (blue) synchronization. The error bars show intermember spread (±1 s.d.). **b**,**c**, As per **a**, but for the 2002–2013 slowdown (**b**) and the 2008–2017 acceleration (**c**).

exhibits even negative trends while the recent acceleration shows large positive trends of almost 0.8 °C per decade. These trends during the cold season are around or out of the ±1 s.d. range of high-synchronization members of the CESM1 large ensemble. The large positive TPI–COWL correlation (red dot in Fig. 3a) explains the strong seasonality in observed trends. Calculations show that the TPI + COWL contribution dominates the seasonality of the three acceleration/slowdown events (Supplementary Fig. 10). Hence, when TPI and COWL are synchronized, acceleration/slowdown events show strong seasonality. The seasonal modulation is another effect of high TEP–COWL synchronization, especially for decade-long events (Fig. 4 and Supplementary Fig. 10).

In summary, we showed that the recent global warming slowdown of 2002–2013 and acceleration of 2008–2017 are strong because the TPI and COWL are in phase and reinforce each other on the rate of GMST increase. The effect of TEP–COWL synchronization is confirmed in strong seasonality of the two events as the COWL is a boreal winter phenomenon. To the extent that the TPI and COWL are physically independent and random-phased, their synchronization appears hard to predict, although there might be some predictability in the Interdecadal Pacific Oscillation[30]. The effect of TPI–COWL synchronization revealed in this study is still useful in diagnosing internal modulations of the rate of GMST increase, an important task given the small and shrinking breathing room from the low-warming targets of the Paris Agreement.

Online content

Any methods, additional references, Nature Research reporting summaries, source data, extended data, supplementary information, acknowledgements, peer review information; details of author contributions and competing interests; and statements of data and code availability are available at https://doi.org/10.1038/s41558-020-0753-9.

Received: 19 February 2019; Accepted: 16 March 2020;
Published online: 20 April 2020

References

1. Trenberth, K. E. Has there been a slowdown? *Science* **349**, 691–692 (2015).
2. Kosaka, Y. & Xie, S.-P. The tropical Pacific as a key pacemaker of the variable rates of global warming. *Nat. Geosci.* **9**, 669–673 (2016).
3. Dong, L. & McPhaden, M. J. The role of external forcing and internal variability in regulating global mean surface temperatures on decadal timescales. *Environ. Res. Lett.* **12**, 034011 (2017).
4. Chen, X. & Tung, K.-K. Global surface warming enhanced by weak Atlantic overturning circulation. *Nature* **559**, 387–391 (2018).
5. Kosaka, Y. & Xie, S.-P. Recent global-warming slowdown tied to equatorial Pacific surface cooling. *Nature* **501**, 403–407 (2013).
6. England, M. H. et al. Recent intensification of wind-driven circulation in the Pacific and the ongoing warming slowdown. *Nat. Clim. Change* **4**, 222–227 (2014).
7. Dai, A., Fyfe, J. C., Xie, S.-P. & Dai, X. Decadal modulation of global surface temperature by internal climate variability. *Nat. Clim. Change* **5**, 555–559 (2015).
8. Meehl, G. A., Hu, A., Santer, B. D. & Xie, S.-P. Contribution of the Interdecadal Pacific Oscillation to twentieth-century global surface temperature trends. *Nat. Clim. Change* **6**, 1005–1008 (2016).
9. Wallace, J., Zhang, Y. & Renwick, J. Dynamic contribution to hemispheric mean temperature trends. *Science* **270**, 780–783 (1995).
10. Molteni, F., Farneti, R., Kucharski, F. & Stockdale, T. N. Modulation of air–sea fluxes by extratropical planetary waves and its impact during the recent surface warming slowdown. *Geophys. Res. Lett.* **44**, 1494–1502 (2017).
11. Li, C., Stevens, B. & Marotzke, J. Eurasian winter cooling in the warming slowdown of 1998–2012. *Geophys. Res. Lett.* **42**, 8131–8139 (2015).
12. Deser, C., Guo, R. & Lehner, F. The relative contributions of tropical Pacific sea surface temperatures and atmospheric internal variability to the recent global warming slowdown. *Geophys. Res. Lett.* **44**, 7945–7954 (2017).
13. Huang, J., Xie, Y., Guan, X., Li, D. & Ji, F. The dynamics of the warming slowdown over the Northern Hemisphere. *Clim. Dynam.* **48**, 429–446 (2017).
14. Sigmond, M. & Fyfe, J. C. Tropical Pacific impacts on cooling North American winters. *Nat. Clim. Change* **6**, 970–974 (2016).
15. Johnson, N. C., Xie, S.-P., Kosaka, Y. & Li, X. Increasing occurrence of cold and warm extremes during the recent global warming slowdown. *Nat. Commun.* **9**, 1724 (2018).
16. Karl, T. R. et al. Possible artifacts of data biases in the recent global surface warming slowdown. *Science* **348**, 1469–1472 (2015).
17. Santer, B. D. et al. Volcanic contribution to decadal changes in tropospheric temperature. *Nat. Geosci.* **7**, 185–189 (2014).
18. Thompson, D., Kennedy, J., Wallace, J. & Jones, P. A large discontinuity in the mid-twentieth century in observed global-mean surface temperature. *Nature* **453**, 646–649 (2008).

19. Broccoli, A. J., Lau, N. C. & Nath, M. J. The cold ocean–warm land pattern: model simulation and relevance to climate change detection. *J. Clim.* **11**, 2743–2763 (1998).
20. Wang, C.-Y., Xie, S.-P., Kosaka, Y., Liu, Q. & Zheng, X.-T. Global influence of tropical Pacific variability with implications for global warming slowdown. *J. Clim.* **30**, 2679–2695 (2017).
21. Zhao, P., Yang, S., Jian, M. & Chen, J. Relative controls of Asian–Pacific summer climate by Asian land and tropical–North Pacific sea surface temperature. *J. Clim.* **24**, 4165–4188 (2011).
22. Mori, M., Kosaka, Y., Watanabe, M., Nakamura, H. & Kimoto, M. A reconciled estimate of the influence of Arctic sea-ice loss on recent Eurasian cooling. *Nat. Clim. Change* **9**, 123–129 (2019).
23. Kay, J. E. et al. The Community Earth System Model (CESM) large ensemble project: a community resource for studying climate change in the presence of internal climate variability. *Bull. Am. Meteorol. Soc.* **96**, 1333–1349 (2015).
24. Power, S., Casey, T., Folland, C., Colman, A. & Mehta, V. Interdecadal modulation of the impact of ENSO on Australia. *Clim. Dynam.* **15**, 319–324 (1999).
25. Taylor, K. E., Stouffer, R. J. & Meehl, G. A. An overview of CMIP5 and the experiment design. *Bull. Am. Meteorol. Soc.* **93**, 485–498 (2012).
26. Zhang, R., Delworth, T. L. & Held, I. M. Can the Atlantic Ocean drive the observed multidecadal variability in Northern Hemisphere mean temperature? *Geophys. Res. Lett.* **34**, L02709 (2007).
27. Cohen, J. L., Furtado, J. C., Barlow, M., Alexeev, V. A. & Cherry, J. E. Asymmetric seasonal temperature trends. *Geophys. Res. Lett.* **39**, L04705 (2012).
28. Saffioti, C., Fischer, E. M. & Knutti, R. Contributions of atmospheric circulation variability and data coverage bias to the warming slowdown. *Geophys. Res. Lett.* **42**, 2385–2391 (2015).
29. Trenberth, K. E., Fasullo, J. T., Branstator, G. & Phillips, A. S. Seasonal aspects of the recent pause in surface warming. *Nat. Clim. Change* **4**, 911–916 (2014).
30. Meehl, G. A., Hu, A. & Teng, H. Initialized decadal prediction for transition to positive phase of the Interdecadal Pacific Oscillation. *Nat. Commun.* **7**, 11718 (2016).

Methods

Observational datasets. We use gridded monthly surface temperature datasets of GISTEMP[31] and BEST (Berkeley Earth Surface Temperatures)[32]. The result of BEST is similar to GISTEMP (not shown). For boreal cold season-mean (warm season-mean, annual-mean), only a grid point that has successive data from 1921 to 2018 with at least one month in each year is used, while the others are treated as missing values. GMST is calculated using these non-missing values. Compared with other surface temperature data, the datasets used in this study have relatively large data coverage defined by non-missing values. We also use atmospheric variables (sea level pressure, 500 hPa and 1,000 hPa geopotential height, 10 m wind vector and 2 m air temperature) from ERA–20C[33] before 2010 and ERA–Interim[34] from 2011 to 2018.

Model experiments. We use four different experiments.

(1) Pre-industrial (PI) experiment: a 1,800-year CESM1 PI run[23] and a 1,000-year CM2.1 PI run. Radiative forcing is fixed at the level of year 1850 (CESM1) and 1860 (CM2.1).

(2) Historical + RCP (HIST) experiment: 40-member CESM1 HIST runs[23] (large ensemble) extended by RCP8.5 since 2006 and 20-member CM2.1 HIST runs[2] extended by RCP4.5 since 2006; 34 models from CMIP5[25] extended by RCP8.5 with only one ensemble member from each model.

(3) Pacific Ocean–Global Atmosphere (POGA) experiment[5]: ten-member CESM1[35] and ten-member CM2.1[2] POGA simulations. In this experiment, the tropical eastern Pacific sea surface temperature anomaly is nudged to ERSST v.3b[36]. The same radiative forcing as in the HIST experiment is used.

(4) Global Ocean–Global Atmosphere (GOGA) experiment: ten-member CESM1 GOGA ensemble. In this experiment, global sea surface temperature of ERSST v.4[37–39] and sea-ice of HadISST[40] are prescribed. It also uses radiative forcing as in the corresponding HIST experiment.

More details for these model experiments can be found in their respective references.

Decomposition of internal variability. Our TEP–COWL relationship is discussed for the internal component. In observations, for both GMST and gridded data we calculate the radiative component as the linear regression part of observed data against the CMIP5 HIST ensemble mean GMST anomaly[7]. The residual is treated as the internal component. The resultant internal component is similar when using the CESM1 HIST ensemble instead of CMIP5 (Supplementary Fig. 1). In climate models, the HIST (including CMIP5) ensemble mean is subtracted as the radiatively forced component.

Analysis methods. We define the 1975–1998 acceleration[41] and the 2002–2013 slowdown[12]. Some initialized predictions[42,43] and observational studies[44,45] indicate a transition to positive Interdecadal Pacific Oscillation and a new acceleration event most recently. To study this acceleration event, 2008–2017 is selected as an event of at least a decade long, but not overlapping too much with the recent slowdown. However, there is still a six-year overlapping period (2008–2013) between the selected slowdown and acceleration events. To test whether the 2008–2017 acceleration event is strongly influenced by the overlapping period, we calculate the six-year anomaly mean pattern of 2008–2013 internal surface temperature and the four-year mean of 2014–2017. Both the patterns show strong anomalies in the TEP and Northern Hemispheric continents but with reversed sign (not shown). Negative anomalies in the overlapping period and positive anomalies in the non-overlapping period both contribute to the strong warming during the selected period. But comparing with the trend pattern (Fig. 1c), the 2014–2017 mean pattern shows higher correlation ($r^2 = 0.56$) than the 2008–2013 mean pattern ($r^2 = 0.37$). The result changes little when choosing the four-year mean of 2008–2011 for the overlapping period ($r^2 = 0.44$). Hence, for the 2008–2017 acceleration event it is preferable to show the contribution of anomalies during the non-overlapping period (the last four years). Further studies should select a totally independent period from the recent slowdown to analyse the recent acceleration when a longer record is available.

Running trend is calculated using Sen's slope[46]. In Fig. 1e, Supplementary Figs. 3b,d and Supplementary Fig. 7b, we use all available model samples used in this study for calculating the model percentiles. In Fig. 3a–c and Supplementary Fig. 9, linear correlation coefficient is tested by two-tailed Student's t-test and linear regression analysis is tested by F-test. In Supplementary Fig. 7, we use an 11-year window, ten-year Lanczos low-pass filter. A yearly time series using this ten-year low-pass filter will lose its first and last five-year data.

The COWL pattern loadings are defined as[9,18]

$$\mathrm{COWL}(x) = \overline{[T(x,t) - T_{\mathrm{NH}}(t)] \cdot T_{\mathrm{NH}}(t)} \quad (1)$$

where $T(x,t)$ are internal Northern Hemispheric (30°N–90°N) surface temperature anomalies given as a function of space, x, and time, t; $T_{\mathrm{NH}}(t)$ denotes the spatial average of $T(x,t)$; and the overbar denotes the time mean. Then we calculate the corresponding COWL index by projecting $[T(x,t) - T_{\mathrm{NH}}(t)]$ onto COWL loadings. The TPI[20] is defined as the spatial average of internal TEP sea surface temperature anomalies from 15°S to 15°N and 180° eastward to 90°W. We use a two-variant linear regression for decomposing the wintertime internal GMST anomaly with the COWL index and TPI as predictors:

$$\mathrm{GMST}_{\mathrm{internal}} = b_1 \mathrm{COWL} + b_2 \mathrm{TPI} + \mathrm{residual} \quad (2)$$

where b_1 and b_2 are the regression coefficients of the COWL index and TPI, respectively. We call the first and second terms of the right-hand side the COWL- and TPI-related internal GMST variability in the boreal cold season, respectively.

Data availability

GISTEMP is from https://data.giss.nasa.gov/gistemp/; BEST is from http://berkeleyearth.org/data/; ERA–20C and ERA–Interim are from https://apps.ecmwf.int/datasets/; CESM1 PI, HIST, POGA and GOGA runs have been obtained from the Earth System Grid (http://www.earthsystemgrid.org); CMIP5 data have been obtained from https://pcmdi.llnl.gov/?cmip5/; CM2.1 PI, HIST and POGA runs are available upon request.

Code availability

The scripts used to produce the main figures, along with the code for the CM2.1 Pacific pacemaker experiment, are available from the corresponding author upon reasonable request.

References

31. Hansen, J., Ruedy, R., Sato, M. & Lo, K. Global surface temperature change. *Rev. Geophys.* **48**, RG4004 (2010).
32. Rohde, R., Muller, R. A., Jacobsen, R., Muller, E. & Wickham, C. A new estimate of the average earth surface land temperature spanning 1753 to 2011. *Geoinform. Geostat.: An Overview* **1**, 1000101 (2013).
33. Poli, P. et al. ERA–20C: an atmospheric reanalysis of the twentieth century. *J. Clim.* **29**, 4083–4097 (2016).
34. Dee, D. P. et al. The ERA–Interim reanalysis: configuration and performance of the data assimilation system. *Q. J. R. Meteorol. Soc.* **137**, 553–597 (2011).
35. Deser, C., Simpson, I. R., McKinnon, K. A. & Phillips, A. S. The Northern Hemisphere extratropical atmospheric circulation response to ENSO: how well do we know it and how do we evaluate models accordingly? *J. Clim.* **30**, 5059–5082 (2017).
36. Smith, T. M., Reynolds, R. W., Peterson, T. C. & Lawrimore, J. Improvements to NOAA's historical merged land–ocean surface temperature analysis (1880–2006). *J. Clim.* **21**, 2283–2296 (2008).
37. Huang, B. et al. Extended reconstructed sea surface temperature version 4 (ERSST.v4): part I. Upgrades and intercomparisons. *J. Clim.* **28**, 911–930 (2015).
38. Liu, W. et al. Extended reconstructed sea surface temperature version 4 (ERSST.v4): part II. Parametric and structural uncertainty estimations. *J. Clim.* **28**, 931–951 (2015).
39. Huang, B. et al. Further exploring and quantifying uncertainties for Extended Reconstructed Sea Surface Temperature (ERSST) version 4 (v4). *J. Clim.* **29**, 3119–3142 (2016).
40. Rayner, N. A. et al. Global analyses of sea surface temperature, sea ice, and night marine air temperature since the late nineteenth century. *J. Geophys. Res.* **108**, 4407 (2003).
41. Yao, S.-L., Luo, J.-J., Huang, G. & Wang, P. Distinct global warming rates tied to multiple ocean surface temperature changes. *Nat. Clim. Change* **7**, 486–491 (2017).
42. Thoma, M., Greatbatch, R. J., Kadow, C. & Gerdes, R. Decadal hindcasts initialized using observed surface wind stress: evaluation and prediction out to 2024. *Geophys. Res. Lett.* **42**, 6454–6461 (2015).
43. Meehl, G. A., Hu, A., Arblaster, J. M., Fasullo, J. & Trenberth, K. E. Externally forced and internally generated decadal climate variability associated with the Interdecadal Pacific Oscillation. *J. Clim.* **26**, 7298–7310 (2013).
44. Hu, S. & Fedorov, A. V. The extreme El Niño of 2015–2016 and the end of global warming hiatus. *Geophys. Res. Lett.* **44**, 3816–3824 (2017).
45. Su, J., Zhang, R. & Wang, H. Consecutive record-breaking high temperatures marked the handover from hiatus to accelerated warming. *Sci. Rep.* **7**, 43735 (2017).
46. Sen, P. K. Estimates of the regression coefficient based on Kendall's tau. *J. Am. Stat. Assoc.* **63**, 1379–1389 (1968).

Acknowledgements

X.L. was supported by the national key research and development project of China (grant no. 2016YFA0601803), the National Natural Science Foundation of China (grant nos. 41925025 and U1606402) and the Qingdao National Laboratory for Marine Science and Technology (grant no. 2017ASKJ01). J.-C.Y. was supported by the Fundamental Research Funds for the Central Universities (grant no. 202013029) and the National Natural Science Foundation of China (grant no. 41806007). Y.Z. was supported by the China Scholarship Council (grant no. 201706330016). Y.K. was supported by the Japanese

Ministry of Education, Culture, Sports, Science and Technology ('the Integrated Research Program for Advancing Climate Models' and 'the Arctic Challenge for Sustainability' projects), by the Japan Society for the Promotion of Science (grant nos. 18H01278, 19H01964 and 19H05703) and by the Japan Science and Technology Agency (Belmont Forum CRA 'InterDec'). Z.L. was supported by the National Natural Science Foundation of China (grant no. 41806007).

Author contributions

J.-C.Y., X.L., S.-P.X. and Y.Z. conceived the analysis. J.-C.Y. performed the data analysis and prepared all figures. Y.K. ran CM2.1 simulations. Z.L. processed CMIP5 data. All authors wrote and reviewed the manuscript.

Competing interests

The authors declare no competing interests.

Additional information

Supplementary information is available for this paper at https://doi.org/10.1038/s41558-020-0753-9.

Correspondence and requests for materials should be addressed to X.L.

Peer review information *Nature Climate Change* thanks Nicholas Tyrrell and the other, anonymous, reviewer(s) for their contribution to the peer review of this work.

Reprints and permissions information is available at www.nature.com/reprints.